MIMO WIRELESS CHANNELS MADE SIMPLE

Akbar M. Sayeed

Department of Electrical and Computer Engineering
University of Wisconsin-Madison
akbar@engr.wisc.edu, http://dune.ece.wisc.edu

ABSTRACT

Fundamental understanding of the interaction between the signal space and the channel is key to reliable communication. In this paper we propose a virtual channel representation for multi-antenna fading channels that captures the essence of such such interaction in the spatial dimension. The virtual representation describes the channel via spatial basis functions defined by fixed virtual angles. The resulting virtual channel matrix provides a simple geometric interpretation of the scattering environment and clearly reveals the two key factors affecting capacity: the number of parallel channels and the level of diversity. Via the concepts of spatial zooming and aliasing, the virtual representation also provides a transparent interpretation of the effects of antenna spacing on channel statistics and capacity.

1. INTRODUCTION

Antenna arrays hold great promise for bandwidth-efficient communication over the harsh wireless channel. The two main characteristics of fading spatial channels from a communication theoretic viewpoint are the *capacity* and *diversity* afforded by the scattering environment. Recent studies that assume an idealized rich scattering environment indicate a linear increase in capacity with the number of antennas [1, 2]. Physical models (see, e.g., [3]) describe realistic scattering environments and the resulting channel statistics determine capacity and diversity. However, simple rules that capture the effects of scattering and array characteristics on capacity and diversity are difficult to draw in general from existing models.

In this paper, we propose a new intermediate *virtual* channel representation that keeps the essence of physical modeling, provides a tractable *linear* channel characterization, and offers a simple interpretation of the effects of scattering and array characteristics on channel statistics, capacity and diversity [4]. Specifically, the virtual representation describes the channel with respect to fixed spatial basis functions defined by fixed virtual angles. Consider a $Q \times P$ matrix with elements $\{H(m,n)\}$ representing a channel with P transmit and Q receive antennas. For uniformly spaced virtual angles, $\{H(m,n)\}$ are related to the virtual channel coefficients $\{H_V(q,p)\}$ via a two-dimensional Fourier transform:

$$H(m,n) = \frac{1}{\sqrt{PQ}} \sum_{q=-\widetilde{Q}}^{\widetilde{Q}} \sum_{p=-\widetilde{P}}^{\widetilde{P}} H_V(q,p) e^{-j2\pi qm/Q} e^{j2\pi pn/P}, \tag{1}$$

where $0 \le m \le Q-1$, $0 \le n \le P-1$, $\widetilde{Q} = (Q-1)/2$ and $\widetilde{P} = (P-1)/2$. This work studies the structure and statistics of $\{H_V(q,p)\}$ imposed by scattering characteristics.

The deceptively simple Fourier relation (1) yields many useful insights [4]. First, under the assumption of independent path gains, $\{H_V(q,p)\}$ are approximately uncorrelated and $\{H(m,n)\}$ constitute a segment of a wide sense stationary (WSS) process. Second, the virtual representation yields an insightful "imaging" interpretation of the scattering geometry: a realistic channel consisting of a superposition of clusters is represented by the virtual matrix $\boldsymbol{H}_V$ consisting of non-vanishing sub-matrices. Third, $\boldsymbol{H}_V$ clearly reveals the effect of scattering on the two key factors affecting capacity: *the number of parallel channels* and *the level of diversity* associated with each parallel channel. The virtual representation also induces a virtual partitioning of scattering paths that explicitly exposes their contribution to capacity and diversity. Finally, via the concepts of spatial zooming and aliasing, the virtual framework provides a transparent interpretation of the effect of antenna spacing on channel statistics and capacity.

The next section presents a general physical model for spatial MIMO channels and introduces the virtual channel representation. Section 3 summarizes some useful properties of the virtual channel matrix. Section 4 discusses capacity calculations and includes an illustrative example. We refer the reader to [4] for a detailed account of this work.

2. MIMO CHANNEL MODELING

In the absence of noise, the transmitted and received signals are related as

$$\boldsymbol{x} = \boldsymbol{H}\boldsymbol{s} \tag{2}$$

where $\boldsymbol{s}$ is the $P \times 1$ transmitted signal, $\boldsymbol{x}$ is the $Q \times 1$ received signal and $\boldsymbol{H}$ denotes the channel matrix coupling the transmitter and receiver elements. For simplicity of exposition we focus on one-dimensional uniform linear arrays (ULAs) of antennas at the transmitter and receiver and consider far-field scattering. Let d_T and d_R denote the antenna spacing at the transmitter and receiver, respectively. The channel matrix can be described via the array steering and response vectors

$$\boldsymbol{a}_T(\theta_T) = \frac{1}{\sqrt{P}} \left[1,\, e^{-j2\pi\theta_T}, \cdots, e^{-j2\pi(P-1)\theta_T}\right]^T$$

This work was supported in part by the NSF under grants CCR-9875805, ECS-9979408 and CCR-0113385, and the ONR under grant N00014-01-1-0825

$$\boldsymbol{a}_R(\theta_R) \;=\; \frac{1}{\sqrt{Q}}\left[1,\, e^{-j2\pi\theta_R}, \cdots, e^{-j2\pi(Q-1)\theta_R}\right]^T \quad (3)$$

where θ is related to the physical angle ϕ (measured with respect to the horizontal axis as in Figures 1 and 2) as $\theta = d\sin(\phi)/\lambda = \alpha\sin(\phi)$, where λ is the wavelength of propagation, and $\alpha = d/\lambda$ is the normalized antenna spacing. The above relation defines a one-to-one map between $-\pi/2 \le \phi < \pi/2$ and $-\alpha \le \theta < \alpha$. However, the steering and response vectors in (3) are periodic in θ with period 1. We consider the principal period $[-0.5, 0.5)$ for θ. This implies that for $\alpha > 0.5$, scatterers outside the range $\phi \in [-\sin^{-1}(0.5/\alpha), \sin^{-1}(0.5/\alpha))$ alias into the principle period for θ. This observation is fundamental to understanding the effect of antenna spacing on capacity.

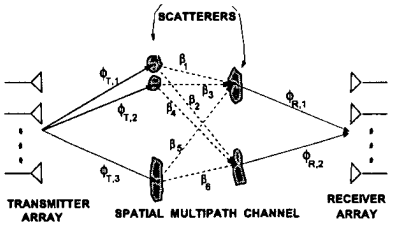

Fig. 1. *A schematic illustrating* **physical** *modeling. Each scattering path is associated with a fading gain (β_l) and a unique pair of transmit and receive angles ($\phi_{T,l}$, $\phi_{R,l}$) corresponding to the scatterers.*

Figure 1 illustrates a widely used *discrete* physical model

$$\boldsymbol{H} = \sum_{l=1}^{L} \beta_l \boldsymbol{a}_R(\theta_{R,l})\boldsymbol{a}_T^H(\theta_{T,l}) \quad (4)$$

which corresponds to signal propagation along L paths with $\{\theta_{T,l} \in S_T\}$ and $\{\theta_{R,l} \in S_R\}$ as the angles seen by the transmitter and receiver, respectively, and $\{\beta_l\}$ as the corresponding independent path gains. The angles lie within the angular spreads S_T and S_R seen by the transmitter and receiver, respectively. Note that (4) is non-linear in the spatial angles.

2.1. Virtual Channel Representation

The finite dimensionality of the spatial signal space can be exploited to develop a *linear virtual* channel representation which uses spatial beams in *fixed virtual* directions. Without loss of generality, assume that P and Q are odd and define: $\widetilde{Q} = (Q-1)/2$ and $\widetilde{P} = (P-1)/2$. The *virtual* representation, illustrated in Figure 2, is given by

$$\boldsymbol{H} = \sum_{q=-\widetilde{Q}}^{\widetilde{Q}} \sum_{p=-\widetilde{P}}^{\widetilde{P}} H_V(q,p)\boldsymbol{a}_R(\tilde{\theta}_{R,q})\boldsymbol{a}_T^H(\tilde{\theta}_{T,p}) = \widetilde{\boldsymbol{A}}_R \boldsymbol{H}_V \widetilde{\boldsymbol{A}}_T^H \quad (5)$$

where $\{\tilde{\theta}_{R,q}\}$ and $\{\tilde{\theta}_{T,p}\}$ are fixed virtual angles that result in full-rank matrices $\widetilde{\boldsymbol{A}}_R = [\boldsymbol{a}_R(\tilde{\theta}_{R,-\widetilde{Q}}), \cdots, \boldsymbol{a}_R(\tilde{\theta}_{R,\widetilde{Q}})]$ $(Q \times Q)$ and $\widetilde{\boldsymbol{A}}_T = [\boldsymbol{a}_T(\tilde{\theta}_{T,-\widetilde{P}}), \cdots, \boldsymbol{a}_T(\tilde{\theta}_{T,\widetilde{P}})]$ $(P \times P)$. The $Q \times P$ matrix $\boldsymbol{H}_V$ is the virtual channel representation. In contrast to (4), the virtual representation is *linear* and is characterized by $\boldsymbol{H}_V$ ($\widetilde{\boldsymbol{A}}_R$ and $\widetilde{\boldsymbol{A}}_T$ are fixed).

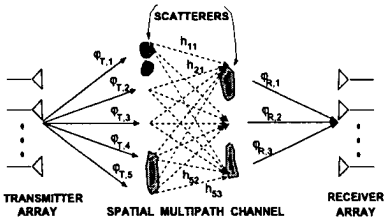

Fig. 2. Virtual *representation of the environment depicted in Figure 1. The virtual angles are fixed a priori and their spacing defines the spatial resolution. The channel is characterized by the virtual coefficients, $\{H_V(q,p) = h_{q,p}\}$, that couple the P virtual transmit angles, $\{\varphi_{T,p}\}$, with the Q virtual receive angles, $\{\varphi_{R,q}\}$.*

Uniform sampling of $\theta \in [-0.5, 0.5)$ is a natural choice for virtual spatial angles: $\tilde{\theta}_{R,q} = q/Q$, $-\widetilde{Q} \le q \le \widetilde{Q}$, $\tilde{\theta}_{T,p} = p/P$, $-\widetilde{P} \le p \le \widetilde{P}$, which results in the steering/response vectors (3) being sinusoids with frequencies $\tilde{\theta}_{T,p}/\tilde{\theta}_{R,q}$, and yields Discrete Fourier Transform matrices $\widetilde{\boldsymbol{A}}_R$ and $\widetilde{\boldsymbol{A}}_T$ (see (1)).

3. PROPERTIES OF VIRTUAL REPRESENTATION

In this section we discuss some important properties of $\boldsymbol{H}_V$ that are insightful in assessing channel statistics, capacity and diversity afforded by a physical scattering environment.

3.1. Virtual Path Partitioning

$\{H_V(q,p)\}$ are related to the physical model (4) as

$$H_V(q,p) = \sum_{l=1}^{L} \beta_l f_Q(\theta_{R,l} - q/Q) f_P^*(\theta_{T,l} - p/P) \quad (6)$$

where $f_Q(\theta) = (1/Q)e^{-j2\pi\theta\widetilde{Q}}\sin(\pi Q\theta)/\sin(\pi\theta)$. We note that the kernel $f_Q(\theta_R)f_P^*(\theta_T)$ peaks at $\theta_R = \theta_T = 0$ and the peak gets sharper with increasing P and Q. The virtual representation induces a partitioning of paths indices in (6) that explicitly exposes the contribution of paths to $\{H_V(q,p)\}$ and to the resulting channel statistics, capacity an diversity.

Define the following partition of path indices in (4): $S_{R,q} = \{l : -1/2Q \le \theta_{R,l} \bmod 1 - q/Q < 1/2Q\}$, $-\widetilde{Q} \le q \le \widetilde{Q}$, and $S_{T,p} = \{l : -1/2P \le \theta_{T,l} \bmod 1 - p/P < 1/2P\}$, $-\widetilde{P} \le p \le \widetilde{P}$, where $\theta \bmod 1$ denotes the value of θ in the principle range $[-0.5, 0.5)$. $S_{R,q}$ is the set of all paths whose receive angles $\theta_{R,l}$ (after shifting them into the principle θ range) are within $1/2Q$ of the q^{th} virtual receive angle $\tilde{\theta}_{R,q} = q/Q$. $S_{T,p}$ is similarly defined with respect to virtual transmit angles. Note that $\bigcup_q S_{R,q} = \bigcup_p S_{T,p} = \bigcup_{p,q}[S_{R,q} \cap S_{T,p}] = \{1, 2, \cdots, L\}$. With the above partitioning (6) can be approximated as

$$H_V(q,p) \approx \sum_{l \in S_{R,q} \cap S_{T,p}} \beta_l \quad (7)$$

which states that the scattering contribution to the virtual angle pair $(q/Q, p/P)$ (and hence $H_V(q,p)$) is proportional to the number of paths whose angles $(\theta_{R,l}, \theta_{T,l})$ lie in the rectangular *virtual spatial bin* of size $1/Q \times 1/P$ centered on $(q/Q, p/P)$: $B_{q,p} =$

$\{(\theta_R, \theta_T) : -1/2Q \leq \theta_R - q/Q < 1/2Q,\ -1/2P \leq \theta_T - p/P < 1/2P\}$. We say that two paths are *distinct* if they can be distinguished in either transmit *or* receive virtual angles; that is, they belong to distinct sets $S_{R,q}$ *or* $S_{T,q}$. We say that two paths are *strictly distinct* if they can be distinguished in both transmit *and* receive virtual angles; that is, they belong to distinct sets $S_{R,q}$ *and* $S_{T,p}$, or, equivalently, their transmit/receive angles lie in distinct bins $B_{q,p}$.

3.2. Statistics of Virtual Channel Coefficients

Using (1), we can explicitly relate the statistics of $\boldsymbol{H}$ and $\boldsymbol{H}_V$ as

$$\begin{aligned} R_H(m-m', n-n') &= \mathrm{E}[H(m,n)H^*(m',n')] \\ &\approx \frac{1}{PQ}\sum_{-\widetilde{Q}}^{\widetilde{Q}}\sum_{-\widetilde{P}}^{\widetilde{P}} \mathrm{E}[|H_V(q,p)|^2] \\ &\quad e^{-j2\pi q(m-m')/Q} e^{j2\pi p(n-n')/P} \end{aligned} \quad (8)$$

since from (7) we have

$$\mathrm{E}[H_V(q,p)H_V^*(q',p')] \approx \left[\sum_{l \in S_{R,q} \cap S_{T,p}} \sigma_l^2\right] \delta_{p-p'}\delta_{q-q'} \quad (9)$$

which uses $\mathrm{E}[\beta_l \beta_{l'}^*] = \sigma_l^2 \delta_{l-l'}$. Thus, under the assumption of independent path gains, $\{H_V(q,p)\}$ are approximately uncorrelated, $\{H(m,n)\}$ form a segment of a WSS process and (8) is analogous to the relationship between the correlation function and power spectral density of a WSS process.

3.3. Imaging of Scattering Clusters

Realistic scattering environments can be modeled via a superposition of clusters with limited angular spreads (see, e.g., [5]). $\boldsymbol{H}_V$ provides an intuitively appealing representation for such environments depicted in Figure 3: different clusters correspond to different non-vanishing sub-matrices of $\boldsymbol{H}_V$. Equation (7) forms the basis of this "imaging" interpretation. Furthermore, the non-vanishing elements of $\boldsymbol{H}_V$ are approximately uncorrelated (see (9)). The size of a sub-matrix of $\boldsymbol{H}_V$ is determined by the size of the corresponding cluster and the antenna spacing α. Consider a single cluster with angular spreads $S_R = [S_{R-}, S_{R+}]$ and $S_T = [S_{T-}, S_{T+}]$ in the ϕ domain. The sub-matrix corresponds to $q = Q_-, \cdots, Q_+$ and $p = P_-, \cdots, P_+$ where $Q_- \approx \lfloor \alpha_R Q \sin(S_{R-}) \rfloor$ and $Q_+ \approx \lceil \alpha_R Q \sin(S_{R+}) \rceil$, and similarly $P_- \approx \lfloor \alpha_T P \sin(S_{T-}) \rfloor$ and $P_+ \approx \lceil \alpha_T P \sin(S_{T+}) \rceil$. For a given cluster size, the size of the sub-matrix increases with α.

The imaging interpretation clearly reveals the two key factors that affect the capacity of each cluster:

- The *number of parallel channels*, PC, which is equal to the rank of the sub-matrix, is determined by the number of transmit and receive virtual angles that lie within the cluster angular spreads.
- The *level of diversity per parallel channel*, D, is determined by the number of virtual receive angles that couple with each virtual transmit angle and vice versa. This depends on the nature of scattering.

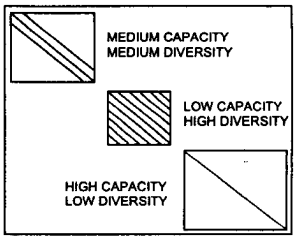

Fig. 3. Decomposition of $\boldsymbol{H}_V$ into non-vanishing sub-matrices corresponding to scattering clusters.

To illustrate how the level of diversity is determined by the nature of scattering let $P = Q$ and consider a single cluster with $S_{R-} = S_{T-} = -\pi/2$ and $S_{R+} = S_{T+} = \pi/2$. On one extreme is "diagonal scattering" ($\boldsymbol{H}_V$ diagonal) in which each transmit virtual angle couples with only one corresponding virtual receive angle resulting in low diversity (largest sub-matrix in Figure 3). On the other extreme is "maximally rich scattering" (all elements of $\boldsymbol{H}_V$ nonzero) in which each virtual transmit angle couples with all virtual receive angles resulting in maximum diversity (smallest sub-matrix in Figure 3). This suggests the following simple k-diagonal virtual model to capture the nature of scattering

$$\boldsymbol{H}_k = \sum_{p=-\widetilde{P}}^{\widetilde{P}} \sum_{q=\max(-\widetilde{P}, p-k)}^{\min(\widetilde{P}, p+k)} H_V(q,p)\boldsymbol{a}_R(\widetilde{\theta}_{R,q})\boldsymbol{a}_T^H(\widetilde{\theta}_{T,p}) \quad (10)$$

where $0 \leq k \leq P-1$. Note that $k = 0$ corresponds to diagonal and $k = P-1$ to maximally rich scattering.

3.4. Spatial Zooming and Aliasing

For given scattering, increasing antenna spacing α decorrelates the channel as well as increases capacity [4]. The effects of *spatial zooming* and *aliasing* are key to this understanding. For simplicity, assume that $\alpha_T = \alpha_R = \alpha$. Consider a cluster with angular spreads in the ϕ domain given by $S_R = [-\Delta\phi_R, \Delta\phi_R]$ and $S_T = [-\Delta\phi_T, \Delta\phi_T]$. The essential effect of increasing α is *spatial zooming*: the antenna array is able to zoom into the cluster in that $\{(\phi_T, \phi_R) \in [-\Delta\phi_T, \Delta\phi_T] \times [-\Delta\phi_R, \Delta\phi_R]\}$ maps to $\{(\theta_T, \theta_R) \in \alpha[-\sin(\Delta\phi_T), \sin(\Delta\phi_T)] \times \alpha[-\sin(\Delta\phi_R), \sin(\Delta\phi_R)]\}$ in the θ domain. Thus, the small cluster in the ϕ domain occupies a larger and larger portion of the θ range as α increases (see Figure 4). Another effect intimately related to zooming is *spatial aliasing*. When the edges of the cluster exceed the principal θ range as α increases, they alias back into the principal range. Both these effect contribute to capacity and diversity since more virtual angles couple with the scatterers as α increases.

4. CAPACITY CALCULATIONS

The number of *parallel channels*, PC, primarily determines the capacity multiplier afforded by multi-antenna systems, and the level of *diversity per parallel channel*, D, primarily determines the slope of the error probability and outage capacity curves. $PC \leq PC_{max} = \min(P, Q)$ and the virtual path partitioning tells us that there have to be at least $L = \min(P, Q)$ *strictly distinct* physical paths to achieve PC_{max}. However, this does not guarantee maximum diversity for each parallel channel. An example

is "diagonal" scattering ($\boldsymbol{H}_0$ in (10)) that achieves PC_{max} but $D = 1$. $D \leq D_{max} = \max(P, Q)$ and if $P \leq Q$, each virtual transmit angle must couple with $D_{max} = Q$ distinct virtual receive angles via *distinct* paths in order to achieve D_{max}. This corresponds to receive diversity. On the other hand, if $P \geq Q$, $D_{max} = P$ distinct virtual transmit angles must couple to each virtual receive angle via *distinct* paths in order to achieve D_{max}. This corresponds to transmit diversity. Thus, we need at least $\min(P, Q) \times \max(P, Q) = PQ$ *strictly distinct* paths to excite all the degrees of freedom in the channel and achieve both PC_{max} and D_{max}. This corresponds to maximally rich scattering ($\boldsymbol{H}_{P-1}$ in (10)).

We present a numerical example in Figure 4 to illustrate the effect of α on capacity for a single $\pi/4 \times \pi/4$-wide (in ϕ domain) cluster. For simplicity, let $P = Q$. Consider the noisy channel, $\boldsymbol{x} = \sqrt{\rho}\boldsymbol{H}\boldsymbol{s} + \boldsymbol{w}$, where ρ is the transmitted power ($\mathrm{E}[\|\boldsymbol{s}\|^2] = 1$) and $\boldsymbol{w}$ is zero-mean complex Gaussian noise vector with $\mathrm{E}[\boldsymbol{w}\boldsymbol{w}^H] = \boldsymbol{I}$. Conditioned on the knowledge of $\boldsymbol{H}$ (or $\boldsymbol{H}_V$) at the receiver, capacity is approximately given by [1, 2]

$$C(\boldsymbol{H}) \approx \log_2 \left[\det\left(\boldsymbol{I} + \rho \boldsymbol{H}_V \boldsymbol{H}_V^H / P\right)\right] \ bits/s/Hz. \quad (11)$$

In Figure 4, $P = Q = 11$ and SNR = $10\log_{10}(\rho)$ = 20dB. Two quantities are plotted for two antenna spacings $\alpha = 0.5, 1.31$. First, a contour plot of $\mathrm{E}[|H_V(p, q)|]^2]$, depicting cluster support in θ, is provided to show the effect of spatial zooming. Second, an outage capacity plot is provided along with the outage capacity of an iid channel (with the same ρ) for comparison. The cluster is simulated via the physical model (4) using $L = 200$ paths and each path is associated with (ϕ_T, ϕ_R) uniformly distributed within the angular spreads. The path gains are simulated as iid zero-mean complex Gaussian random variables and the clustered and iid channels have the same power. The outage capacity plots are computed from 1000 independent channel realizations.

As evident from Figures 4(a) and (c), the effective size of the cluster in the θ domain increases due to spatial zooming as α increases. This is accompanied by a corresponding increase in capacity in Figures 4(b) and (d) due to increase in the number of parallel channels and decorrelation of channel coefficients as more and more virtual angles couple with the scatterers. For $\alpha = 1.31$ the cluster covers the entire θ region, thereby effectively yielding an iid channel as in Figures 4(c) and (d).

5. REFERENCES

[1] G. J. Foschini, "Layered space-time architecture for wireless communication in a fading environment when using multi-element antennas," *Bell Labs Tech. J.*, vol. 1, no. 2, pp. 41–59, 1996.

[2] E. Telatar, "Capacity of multi-antenna gaussian channels," *AT& T-Bell Labs Internal Tech. Memo.*, June 1995.

[3] A. J. Paulraj and C. B. Papadias, "Space-time processing for wireless communications," *IEEE Signal Processing Magazine*, pp. 49–83, Nov. 1997.

[4] A. M. Sayeed, "Deconstructing multi-antenna fading channels," *to appear in the IEEE Trans. Signal Processing*, 2002.

[5] J. Fuhl, A. F. Molisch, and E. Bonek, "Unified channel model for mobile radio systems with smart antennas," *IEE Proc. Radar, Sonar Navig.*, vol. 145, pp. 32–41, Feb. 1998.

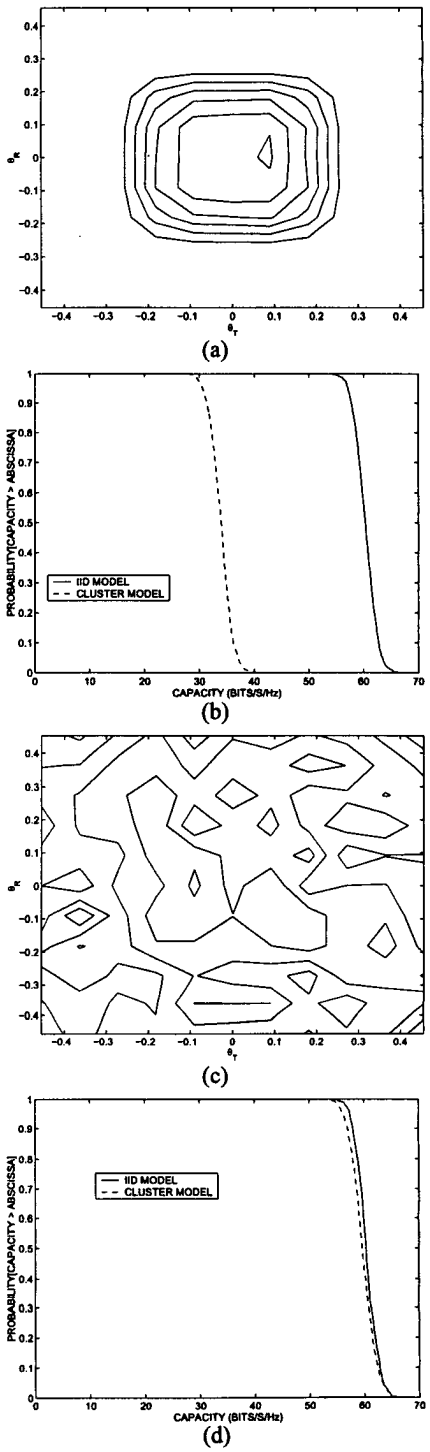

Fig. 4. *Effect of antenna spacing on capacity for a single-cluster environment. Contour plots of* $E[|H_V(q, p)|^2]$ *and outage capacity plots for both the cluster and iid channels are shown. (a) Contour plot of* $E[|H_V(p, q)|^2]$ *for* $\alpha = 0.5$. *(b) Outage capacity plots for* $\alpha = 0.5$. *(c) and (d) correspond to (a) and (b) for* $\alpha = 1.31$. *The cluster and iid channels are identical at* $\alpha = 1.31$ *due to maximum zooming.*